AD-A192 381

AFGL-TR-87-0326

Rocket Measurements Within a Polar
Cap Arc: Ionospheric Modelling

Robert E. Sheehan

Boston College
140 Commonwealth Avenue
Chestnut Hill, MA 02167

19 November 1987

Scientific Report No. 2

APPROVED FOR PUBLIC RELEASE; DISTRIBUTION UNLIMITED

AIR FORCE GEOPHYSICS LABORATORY
AIR FORCE SYSTEMS COMMAND
UNITED STATES AIR FORCE
HANSCOM AIR FORCE BASE, MASSACHUSETTS 01731

88 3 17 060

REPORT DOCUMENTATION PAGE

1a. REPORT SECURITY CLASSIFICATION	1b. RESTRICTIVE MARKINGS
Unclassified	

2a. SECURITY CLASSIFICATION AUTHORITY	3. DISTRIBUTION / AVAILABILITY OF REPORT
	Approved for public release: distribution
2b. DECLASSIFICATION / DOWNGRADING SCHEDULE	unlimited

4. PERFORMING ORGANIZATION REPORT NUMBER(S)	5. MONITORING ORGANIZATION REPORT NUMBER(S)
Report No. 2	AFGL-TR-87-0326

6a. NAME OF PERFORMING ORGANIZATION	6b. OFFICE SYMBOL (If applicable)	7a. NAME OF MONITORING ORGANIZATION
Trustees of Boston College		Air Force Geophysics Laboratory

6c. ADDRESS (City, State, and ZIP Code)	7b. ADDRESS (City, State, and ZIP Code)
140 Commonwealth Avenue Chestnut Hill, MA 02167	Hanscom AFB, MA 01731

8a. NAME OF FUNDING / SPONSORING ORGANIZATION	8b. OFFICE SYMBOL (If applicable)	9. PROCUREMENT INSTRUMENT IDENTIFICATION NUMBER
		F19628-85-K-0051

8c. ADDRESS (City, State, and ZIP Code)	10. SOURCE OF FUNDING NUMBERS			
	PROGRAM ELEMENT NO.	PROJECT NO.	TASK NO.	WORK UNIT ACCESSION NO.
	62101F	4643	08	AI

11. TITLE (Include Security Classification)

Rocket Measurements Within a Polar Cap Arc: Ionospheric Modelling

12. PERSONAL AUTHOR(S)
Robert E. Sheehan

13a. TYPE OF REPORT	13b. TIME COVERED	14. DATE OF REPORT (Year, Month, Day)	15. PAGE COUNT
Scientific Rpt. No. 2	FROM 9-1-86 TO 9-30-87	1987 November 19	34

16. SUPPLEMENTARY NOTATION

17. COSATI CODES			18. SUBJECT TERMS (Continue on reverse if necessary and identify by block number)
FIELD	GROUP	SUB-GROUP	ionospheric model
04	01		polar cap
20	09		F-region auroral arc

19. ABSTRACT (Continue on reverse if necessary and identify by block number)

Precipitating electron fluxes measured over a polar cap, F-region auroral arc were input to an ionospheric model that calculates production rate and density profiles of various species. The model also finds the electron temperature and electric conductivities over a specified altitude range. Most model results compare favorably with rocket measurements taken near apogee over the arc. The actual electron temperature is underestimated by the model and the relative densities of some minor species do not agree. Model results show that initial density conditions in particular strongly affect the development of electron density enhancements produced by dynamic, short lived (15 min) fluxes of soft electrons. The neutral atmosphere chosen for the model also influences the electron density profile produced by soft fluxes. Such differences may play a role in the solar cycle dependence of density fluctuations that cause scintillations in the polar cap.

20. DISTRIBUTION / AVAILABILITY OF ABSTRACT	21. ABSTRACT SECURITY CLASSIFICATION
☐ UNCLASSIFIED/UNLIMITED ☐ SAME AS RPT. ☐ DTIC USERS	Unclassified

22a. NAME OF RESPONSIBLE INDIVIDUAL	22b. TELEPHONE (Include Area Code)	22c. OFFICE SYMBOL
Edward Weber		AFGL/LIS

Acknowledgements

I thank D. Strickland for help in understanding his original model. Data was kindly supplied by W. McMahon (AFGL, electron fluxes), J. Ballenthin (AFGL, absolute and relative density measurements), and P. Rodriguez (NRL, electron temperature measurements). This work was supported by U.S. Air Force contract F19628-85-K-0051.

DTIC COPY INSPECTED 1

iii

TABLE OF CONTENTS

Figure Captions

Figure 1. Flowchart showing the major elements of the ionospheric model.

Figure 2. PIIE observations of electron density fluctuations, total electron density, electron temperature, and energy flux of precipitating electrons vs. time (seconds after launch), altitude, and UT. Vertical line indicates time of the model calculation inside the arc (284 SAL).

Figure 3. Differential flux spectrum of downgoing electrons input to the model corresponding to the time indicated by the vertical line in Figure 2.

Figure 4. Example of typical electron flux observed outside arc.

Figure 5. Model calculations of total electron density, $O+$ density, and electron temperature resulting from the flux in Figure 3.

Figure 6. Hall and Pedersen electric conductivities resulting from the flux in Figure 3.

Figure 7. Relative densities of $N+$, $NO+$, and $O+$ observed during the flight.

Figure 8. Relative densities of N_2+ and O_2+ observed during the flight.

Figure 9. Calculated electron density profiles corresponding to increasing flux duration (c.f. Figure 3).

Figure 10. Same as Figure 9 except starting from a lower initial electron density.

Figure 11. Decay of electron density profile after flux in Figure 2 is turned off.

Figure 12. Development of electron density profile using electron flux outside arc (c.f. Figure 4).

Figure 13. Same as Figure 12 except starting from a lower initial electron density.

Figure 14. Calculated electron density profiles using flux inside arc and a cold neutral atmosphere ($T_n=750K$).

Figure 15. Same as Figure 15 except with a hotter neutral atmosphere ($T_n=1200K$).

1. Introduction

A rocket experiment conducted in Greenland on March 15, 1985, the Polar Ionospheric Irregularities Experiment (PIIE), took detailed measurements of important quantities as it passed over an F-layer polar cap auroral arc. Descriptions of the instruments and observations during the flight can be found in Weber et al. (1987). Data from the mission provided key inputs and valuable checks for an ionospheric model capable of handling soft electron fluxes often seen over polar cap auroral arcs. The original model codes for differential electron flux throughout an ionospheric column (flux transport) were developed by Strickland et al. (1976); local chemistry and O+ diffusion codes were added to find ion densities and optical emissions. This model was used by Weber et al. (1985) to identify the source of F-region plasma enhancements at the equatorward boundary of the auroral zone. Later, we included an electron temperature calculation with heat conduction along magnetic field lines, permitting us to more accurately determine temperature dependent parameters such as chemical rate and O+ diffusion coefficents.

The flowchart in Figure 1 shows the principal features of the model. In its present setup the code has two distinct parts: part 1 in the upper section (transport) calculates production rates of important ion and neutrals that result from a flux of incident electrons at an upper altitude boundary; part 2 uses the production rates to calculate ionospheric densities, temperature, and electric conductivities. The flux transport program requires a neutral atmosphere model consisting of N_2, O_2, and O and a table of cross sections describing important inelastic scattering processes involving electrons and the ambient neutrals.

Strickland et al. (1976) demonstrate how the Boltzmann equation is reduced to a one-dimensional, steady state, transport equation for

differential electron flux over altitude. Scattering terms involve both elastic and inelastic collisions. Since electrons cannot gain energy in the model, no external forces are considered; secondaries are produced isotropically and contribute to the thermal population. Because the flux at a given energy and pitch angle can result only from electrons at the same or higher energies, the code steps successively to lower energies in one pass.

A matrix representation of the transport equation is solved for 20 pitch angles over an energy grid appropriate for the incident differential flux (el/cm-s-sr-ev). An exact eigenvalue solution is found at some intermediate altitude, which leads to solutions at other altitudes from standard perturbation techniques. The code is relatively fast yet more sophisticated than empirical range theoretic models (Rees, 1963). It does not require a matching of solutions between high and low energy ranges as do schemes employing a Fokker-Planck approximation at high energies (Banks et al., 1974). Mantas and Walker (1975) use a similar approach that differs somewhat in the representation of flux vs. energy. An energy conservation test compares the energy lost by the electron flux against the energy expended in ionization and excitation of the neutral constituents.

Chemical production rates and the electron plasma heating rate calculated by the flux transport code become inputs to the ionospheric chemistry and temperature codes in the bottom of Figure 1. These inputs are constant in time but can be switched off to simulate decay in the absence of an ionizing flux. Starting from initial values for the electron temperature and densities of various neutral ionic species, the main chemistry code integrates the chemical rate equations using a predictor-corrector method with an adaptive time step. Because O+ is the only ion appreciably affected by diffusion along magnetic field lines it is handled separately in concert with the other

species. The calculated electron density (total ion density) then determines the electron heat conduction coefficient and the total electron plasma heating rate.

A Crank-Nicolson finite differencing scheme solves both the heat conduction and diffusion equations; the method is implicit, meaning that a solution involves unknown values at adjacent altitudes. Solutions are always stable (Gerald and Wheatley, 1984) but at the price of having to solve a set of simultaneous equations. The diffusion equation is relatively straightforward since the coefficients depend only on temperature and other parameters which are updated at regular time intervals. The temperature, however, requires the solution of a non-linear equation with coefficients that depend on the temperature. With short time steps the problem can be managed by assuring that the coefficients change slowly enough to be linearly projected to the end of each time step. Alternatively, other researchers have used Newton's method to solve a different formulation of the non-linear, diffusion type partial differential equation (Hastings and Roble, 1977; Mantas et al., 1981).

The resulting T_e is then used to recalculate temperature dependent rate coefficients and the O+ diffusion coefficient. The ion temperature, T_i, is not calculated now by the code but is set between the electron and neutral temperatures. Our experience indicates that a loop through the chemistry, diffusion, and temperature codes every second for the first 2 minutes in ionosphere time yields reasonable results. After 2 minutes, when quantities change more slowly, the update time is lengthened to 10 seconds. Pederson and Hall electric conductivities are also calculated from expressions found in Vallence-Jones (1974) with the derived electron temperature and density profiles.

The present model is limited to one dimension along a magnetic field line and neglects horizontal transport. This is adequate to describe an auroral arc several kilometers wide that is either stationary or has its production source moving with the convection velocity. Real physical conditions are more complicated than these simple assumptions; the prime aim of this work is to find out how well the simplified model fares in a carefully documented case study. Other ionospheric models with rather complex chemistry have been developed over the past 15 years (e.g., Jones and Rees, 1963; Roble and Rees, 1977; Schunk et al., 1986). The main advantage of this model centers on the detailed specification of production rates resulting from a measured differential electron flux. Global or limited two dimensional models would require many such calculations in addition to horizontal transport in the chemistry model. A parameterization of the flux transport code to handle many situations is the next logical step in the development of this particular model.

2. PIIE Measurements and Model Results

Figure 2 (Figure 5 from Weber et al. (1987)) displays measurements taken by the instrumented rocket payload as it passed over a complicated system of F-layer auroral arcs near apogee. The vertical line indicates the time chosen for model comparisons. The electron density had a local maximum of 3×10^4 el/cm^3 and T_e was about 3000K at 415 km altitude. Electrons precipitating into the arc carried an energy flux of about .1 erg/cm^{3}s, nearly an order of magnitude greater than in adjacent regions. The differential electron flux spectrum at this time appears in Figure 3. Although only a .5 s average sample, the spectrum is representative of a 5 s interval near the center of the arc. During the time when the rocket was travelling almost horizontally near apogee, one of the electrostatic analyzers sampled pitch angles near 45°. Since there were no measurements taken simultaneously at

4

other pitch angles less than 90° we assumed an isotropic distribution of downgoing electrons. Outside the arc (Figure 4) fluxes were 2 orders of magnitude lower but decreased more gradually at higher energies.

Model results inside the arc (Figure 5) indicate a peak electron density of about 5×10^4 el/cm^3 at 300 km altitude and 3.5×10^4 el/cm^3 at the rocket apogee altitude; T_e at 145 km altitude was calculated to be slightly greater than 2000K. O+ ions dominate at high altitudes but are replaced by increasing amounts of NO+, O$_2$+, N+, and N$_2$+ at lower altitudes. These results start from an initial $n_e = 10^4$ el/cm^3 at all altitudes and $T_e = 3000$K at 600 km altitude, after which production by the precipitating electrons is turned on for 2 minutes. More realistic initial densities estimated from the upleg density profile outside the arc yield somewhat higher densities ($\sim 5 \times 10^4$ el/cm^3). The calculated T_e, however, is not greatly affected when appreciably different initial conditions are used. Hall and Pedersen electric conductivities calculated inside the arc are shown in Figure 6. Even though most ionization occurs above 200 km both conductivities peak low in the E region where collisions with neutrals rapidly increase.

Although the model electron density compares reasonably well with the data, the electron temperature is somewhat lower than measured. Because the only source now incorporated in the model is collisional heating by energetic electrons, this discrepency may in part stem from other types of heating. More fundamentally, heat conduction is only part of the full energy balance equation (Schunk and Walker; 1970); terms representing other forms of heat transport could modify the results. For example, Schunk et al. (1987) demonstrate that thermoelectric cooling by field-aligned currents becomes significant only for rather large return currents of thermal electrons on the order of 10 μA/m2. Weber et al. (1987) estimate maximum field-aligned

currents of ~5 $\mu A/m^2$ within the arc, suggesting a minimal contribution from this effect.

Relative densities of several ionic species can also be compared with model results. Figures 7 and 8 show ion currents for several species measured by the ion mass spectrometer. Since the current is proportional to the ion density, relative densities of the species can be computed. Density ratios of $O+/N+$ and $N+/NO+$ were about 10 to 1 and 3 to 1, respectively. With an initial profile containing only only $O+$ (= 1×10^4 cm^{-3} at all altitudes) the corresponding model ratios after 2 min are close to the measured ones. With a more realistic initial profile ($O+$ = 1.13×10^4, $NO+$ = 1.42×10^3, O_2+ = 7.41×10^2, $N+$ = 3.43×10^1, and N_2+ = 9.59×10^0 cm^{-3}, all at 400 km), $O+/N+$ = 12 and $N+/NO+$ = 1.2 after 2 min. While the total ion density and $O+/N+$ ratio at 400 km are relatively insensitive to initial conditions, other minor species show greater dependence on initial densities, especially several minutes after t = 0. For example, Figure 8 indicates that O_2+ dominates N_2+ at 400 km while the model has N_2+ = 1.02×10^3 and O_2+ = 5.48×10^1 cm^{-3} when $O+$ is the only species initially present. The realistic initial condition leads to N_2+ = 9.51×10^2 and O_2+ = 6.26×10^2 cm^{-3}, a much closer correspondence.

3. Discussion

Densities associated with an arc lasting a few minutes to several tens of minutes depend both on the initial ionosphere and the duration of enhanced production. Although direct procuction by precipitating electrons leads to a rapid buildup of ionization, equilibrium resulting from chemistry and diffusion is reached slowly (several tens of minutes in the F-region vs.

minutes in the E-region). Starting with rather artificial initial conditions, the next two examples (Figures 9 and 10) illustrate how the electron density profile develops when a flux like that observed during PIIE is turned on continuously for 30 minutes.

In Figure 9, O+ ions alone are present initially with a constant height profile of 10^4 cm^{-3}. From 120 to 200 km altitude production and loss quickly balance and equilibrium densities are reached after 10 minutes or so. Below 120 km production is slight and the density actually decreases. Ion production dominates above 200 km, causing a steady increase in electron density that is limited by O+ diffusion until equilibrium is reached several hours later. Starting with an O+ density of 10^3 cm^{-3}, Figure 10 indicates that the final density profile after 30 minutes is not different than seen in Figure 8, except at the lowest altitudes. From 130 to 200 km the equilibrium densities are nearly equal; above 200 km the profiles are similar but lag behind those in Figure 8 because of the smaller initial density. However, on time scales longer than 5 minutes, the resulting densities above 100 km agree to within 20% even when drastically different initial conditions are assumed.

Figure 11 shows what happens if the flux is turned on for 15 minutes and then suddenly switched off, after which direct production ceases and ionization decays, subject only to local chemistry and diffusion. Following an abrupt drop caused by rapid losses, the electron density slowly decays, especially at and above the altitude peak. Here diffusion flattens the profile and maintains the density above 400 km where losses by recombination are minimal.

For comparison, Figures 12 and 13 show electron density profiles generated by fluxes measured outside the main auroral arc at about 306 sec into the flight (Figure 4). Initial O+ densities are 10^4 and 10^3 cm^{-3} as

before. Here the initial density conditions clearly affect the profiles even after several minutes have elapsed. Only in the E-region where local chemistry is relatively fast do the densities approach the same equilibrium, and neither case approximates the densities observed in the downleg segment. Since the electron energy flux measured from 420 km to 290 km nowhere approaches the more energetic flux seen earlier, it seems likely that the observed electron density results from a combination of ionization remaining after local production ceased and that brought in by convection.

A future goal of this study is to find the relationship between large scale features in the polar cap ionosphere and scintillations of satellite to radio transmissions. Scintillations are caused by plasma density irregularities with scale sizes from 100 m to 10 km (Weber and Bachau, 1985). These irregularities have been associated with plasma instabilities generated by density gradients in enhanced plasma regions (blobs) hundreds of km across or with velocity shears (Basu et al., 1986). Hence, density features resulting from direct production or transport play an important role in the problem. For example, observed changes in scintillation behavior with the solar cycle (Aarons, 1982) may be connected with the way these features are generated. A model can probe how similar fluxes affect neutral atmospheres with different exospheric temperatures. In Figure 14, a cold atmosphere like that found during solar minimum produces a slightly higher density at lower altitudes (cf. Figure 9, T_{exo} = 1000K). A hot neutral atmosphere has peak density above 300 km and a more gradual decrease toward higher altitudes (Figure 15). Differences between profiles may help identify which processes generate irregulatities and the scale sizes likely to be observed.

References

Aarons, Jules, Global morphology of ionospheric scintillations, Proc. IEEE, 70, 360, 1982.

Banks, P.M., Chapell, C.R., and A.F. Nagy, A new model for the interaction of auroral electrons with the atmosphere: spectral degradation, backscatter, optical emission, and ionization, J. Geophys. Res., 79, 1459, 1974.

Basu, Sunanda, Basu, Santimay, Senior, C., Weimar, D., Nielsen, E., and P.F. Fougere, Velocity shears and sub-km scale irregularities in the nighttime auroral F-region, Geophys. Res. Lett., 13, 101, 1986.

Gerald, Curtis F., and Patrick O. Wheatley, Applied Numerical Analysis, Third edition, Addison-Wesley Publishing Co., Reading, MA, 1984.

Hastings, J.T., and R.G. Roble, An automatic technique for solving coupled vector systems of non-linear parabolic partial differential equations in one space dimension, Planet. Space Sci., 25, 209, 1977.

Jones, R.A., and M.H. Rees, Time dependent studies of the aurora 1. ion density and composition, Planet. Space Sci., 21, 537, 1973.

Mantas, George P., and James C.G. Walker, The penetration of soft electrons into the ionosphere, Planet. Space Sci., 24, 409, 1975.

Mantas, George P., Carlson, Herbert C. Jr., and Caesar H. LaHoz, Thermal response of the F region ionosphere in artificial modification experiments by hf radio waves, J. Geophys. Res., 86, 561, 1981.

Roble, R.G., and M.H. Rees, Time-dependent studies of aurora: effects of particle precipitation on the dynamic morphology of ionospheric and atmospheric properties, Planet. Space Sci., 25, 991, 1977.

Rees, M.H., Auroral ionization and excitation by incident energetic electrons, Planet. Space Sci., 11, 1209, 1963.

Schunk, Robert W., and James C.G. Walker, Thermal diffusion in the F2-region of the ionosphere, Planet. Space Sci., 18, 535, 1970.

Schunk, R.W., Sojka, J.J., and M.D. Bowline, Theoretical study of the electron temperature in the high-latitude ionosphere for solar maximum and winter conditions, J. Geophys. Res., 91, 12041, 1986.

Schunk, R.W., Sojka, J.J., and M.D. Bowline, Theoretical study of the effect of ionospheric return currents on the electron temperature, J. Geophys. Res., 92, 6013, 1987.

Strickland, D.J., Book, D.L., Coffey, T.P., and J.A. Fedder, Transport equation techniques for the deposition of auroral electrons, J. Geophys. Res., 81, 2755, 1976.

Vallance Jones, Alister, Aurora, D. Reidel Publishing Co. Inc., Boston, 1974.

Weber, E.J., and J. Buchau, Observations of plasma structure and transport at high latitudes, in the Polar Cusp, p. 279, ed. by J.A. Hottet and A. Egeland, D. Reidel Publishing Co. Inc., Boston, 1985.

Weber, E.J. Tsunoda, R.T. Buchau, J., Sheehan, R.E., Strickland, D.J., Whiting, W., and J.G. Moore, Coordinated Measurements of auroral zone plasma enhancements, J. Geophys. Res., 90, 6497, 1985.

Weber, E.J., Kelley, M.C., Ballenthin, J.O., Basu, S., Carlson, H.C., Fleischman, J.R., Hardy, D.A., Maynard, N.C., Pffaf, R.F., Rodriguez, P.A., Sheehan, R.E., and M. Smiddy, Rocket measurements within a polar cap arc: plasma, particle, and electric circuit parameters, submitted to J. Geophys. Res., 1987.
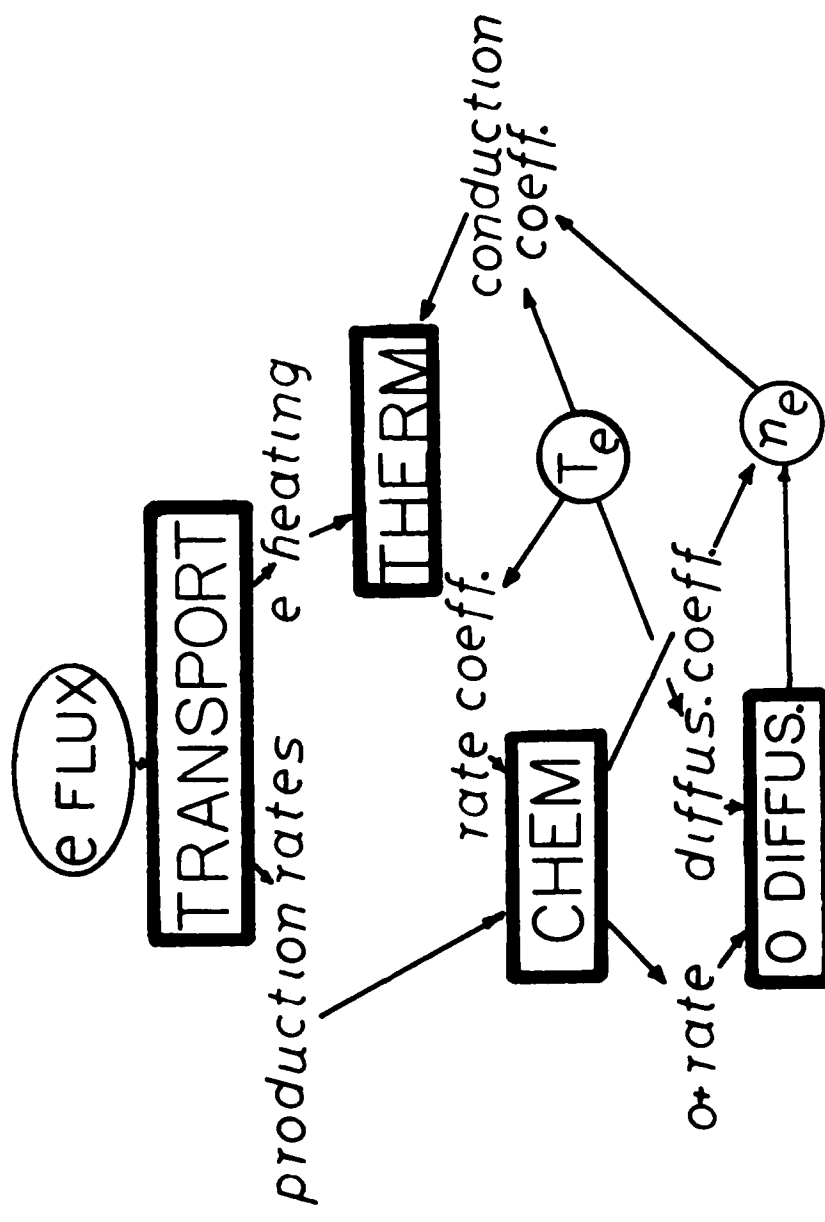
Figure 1
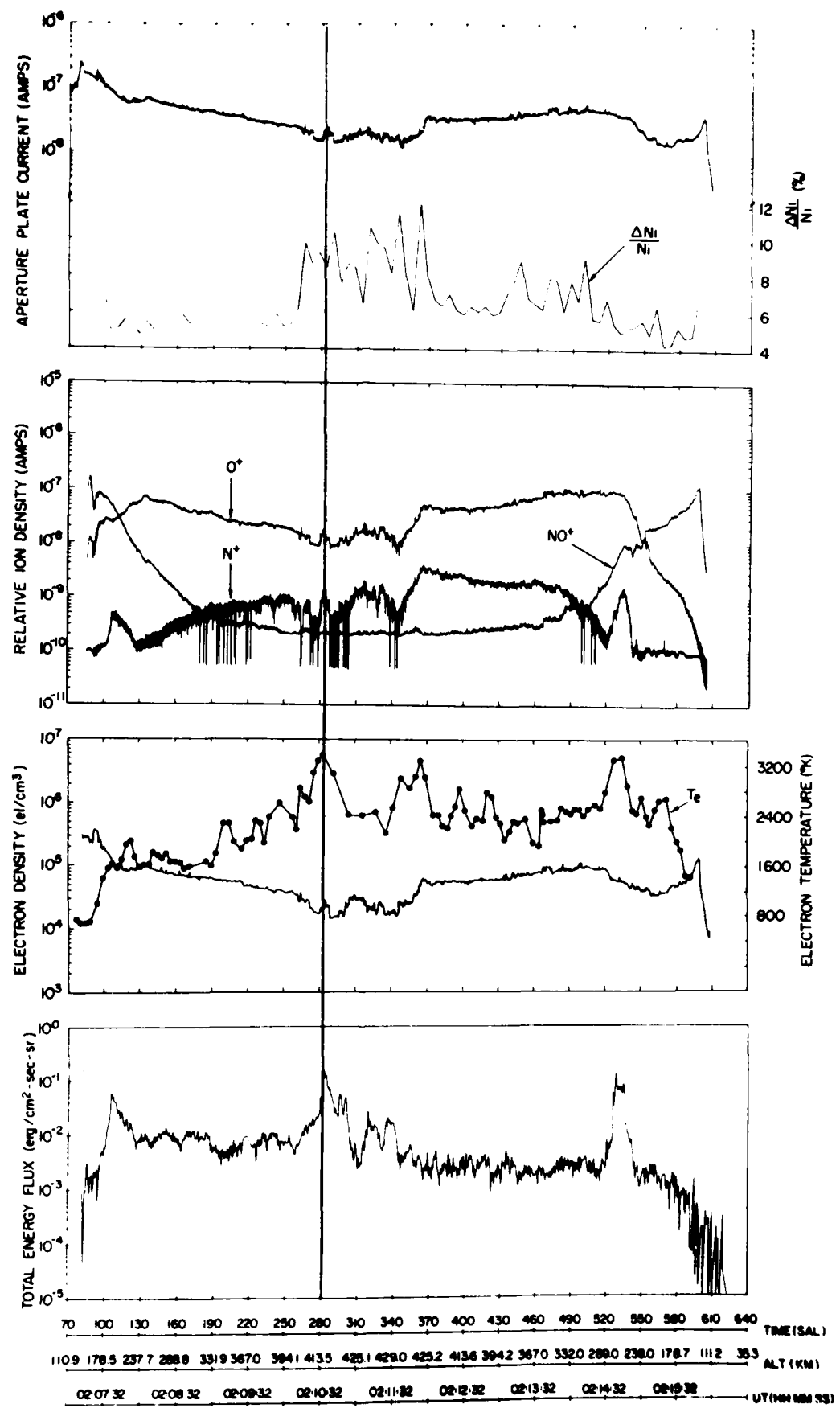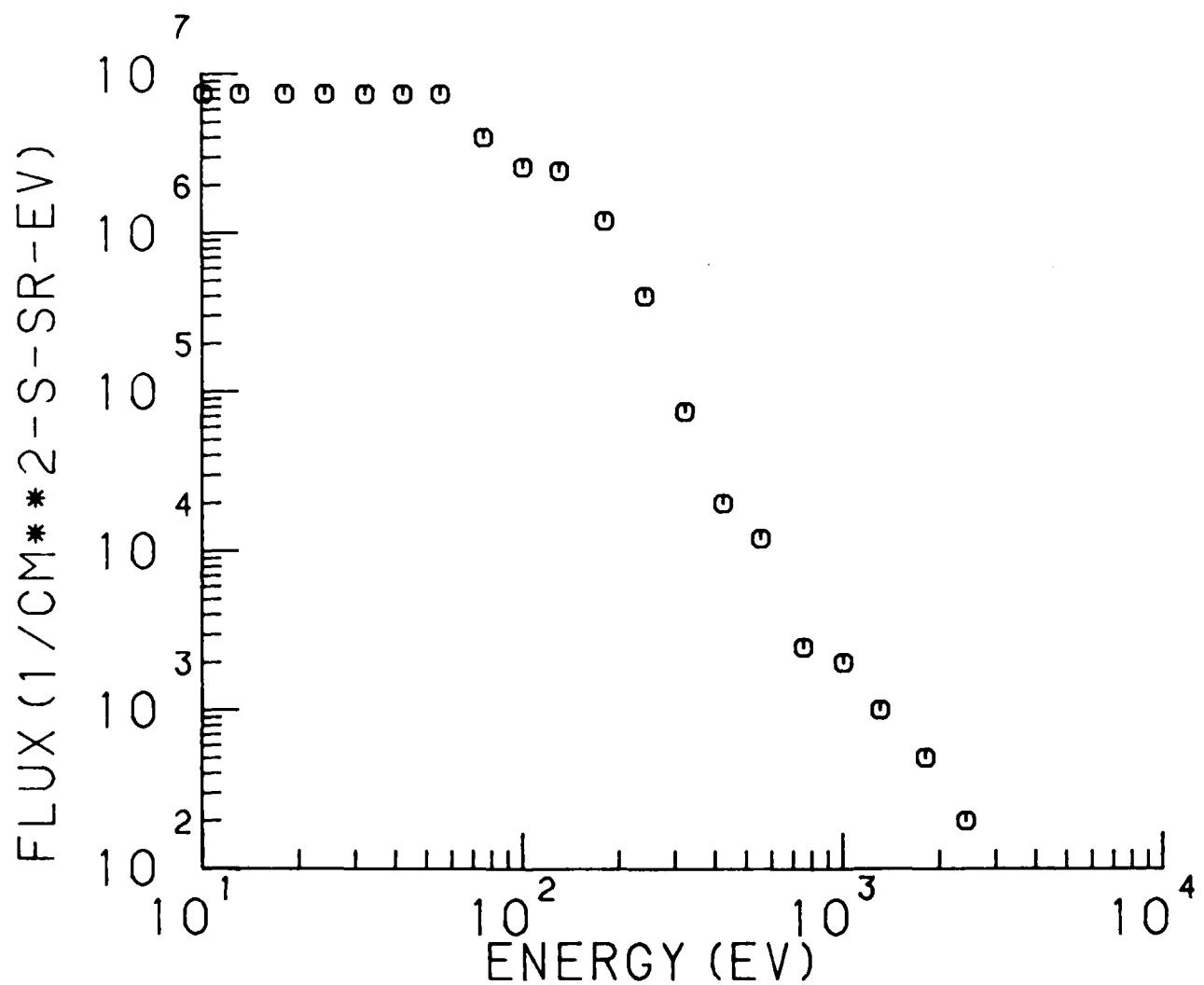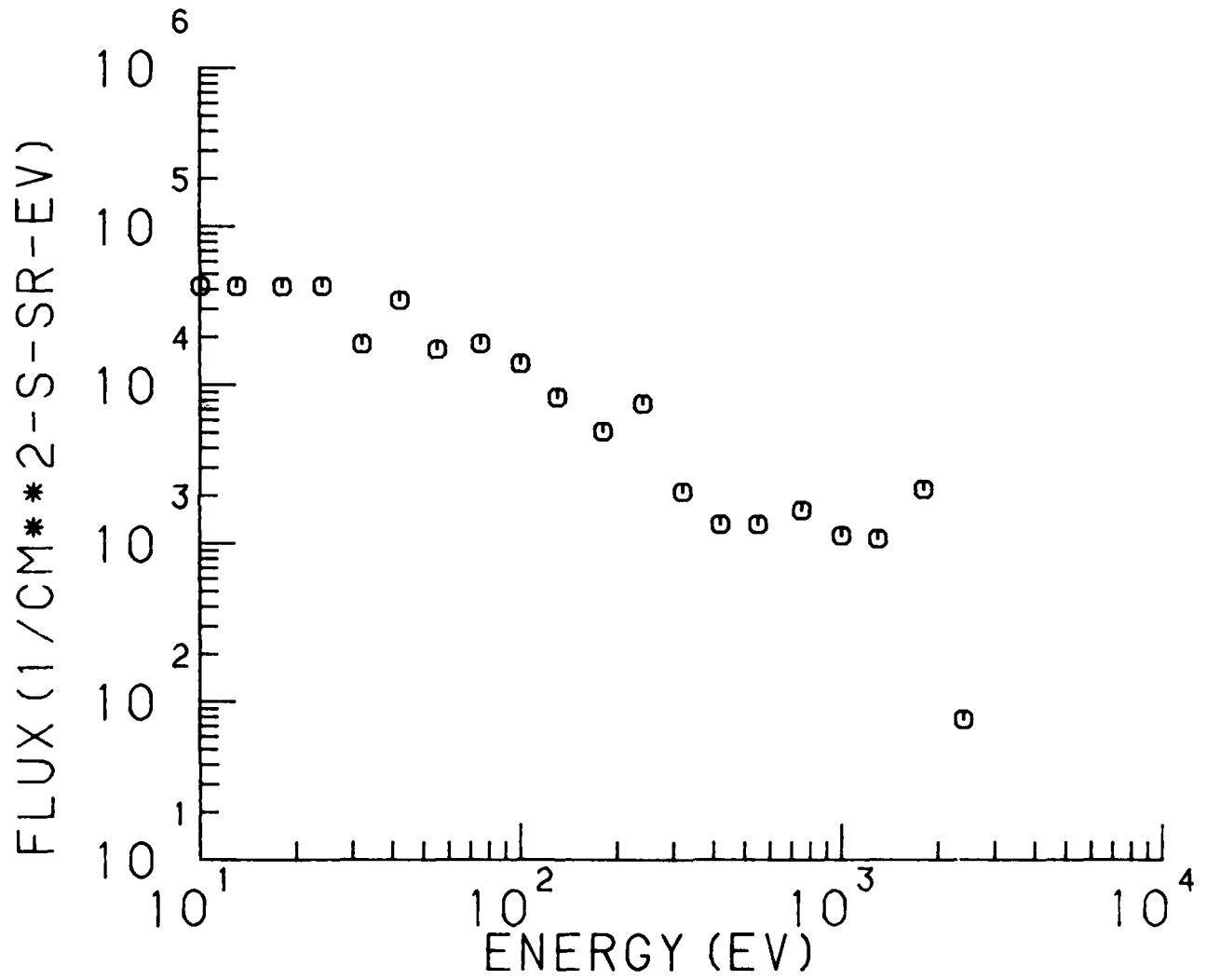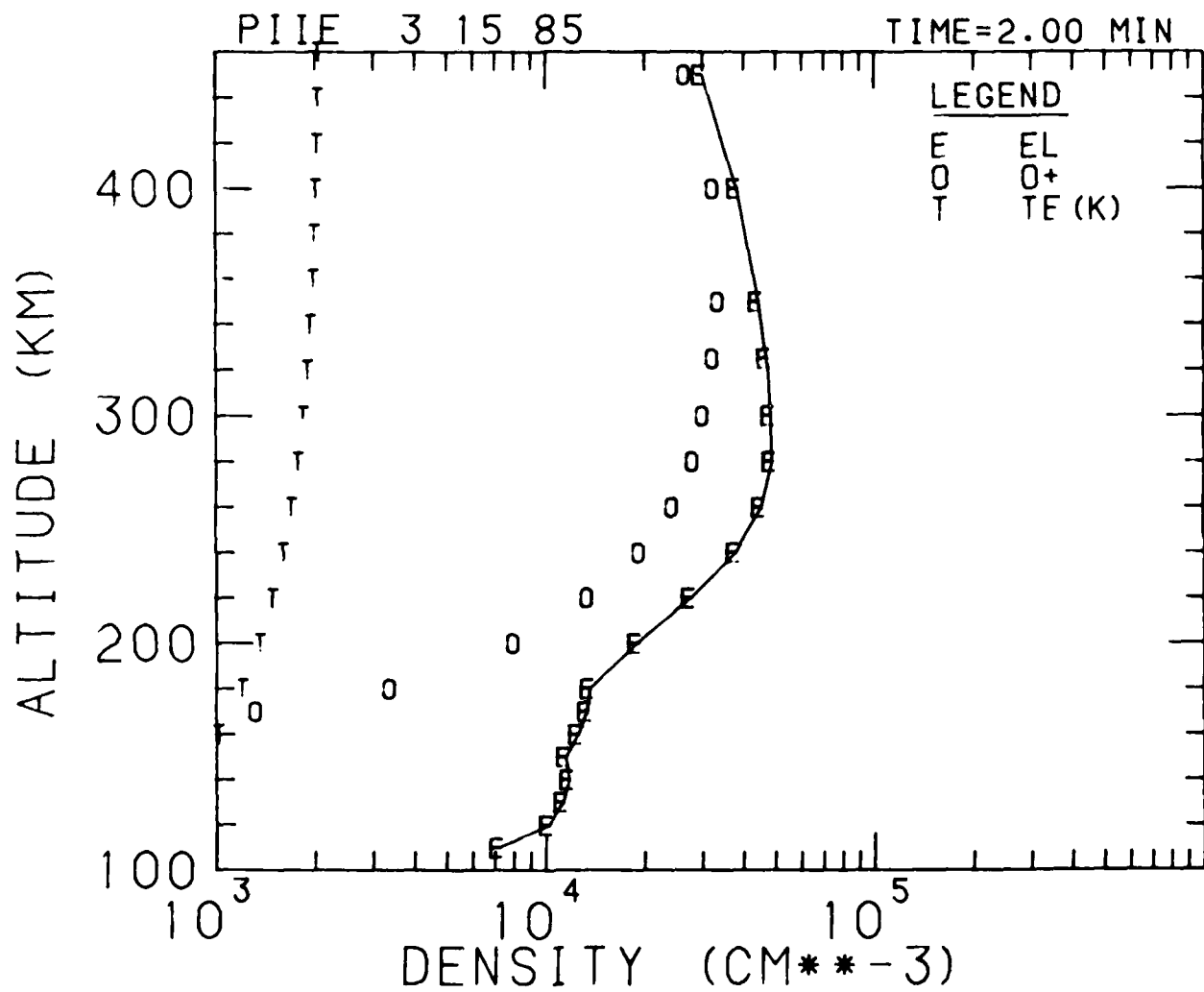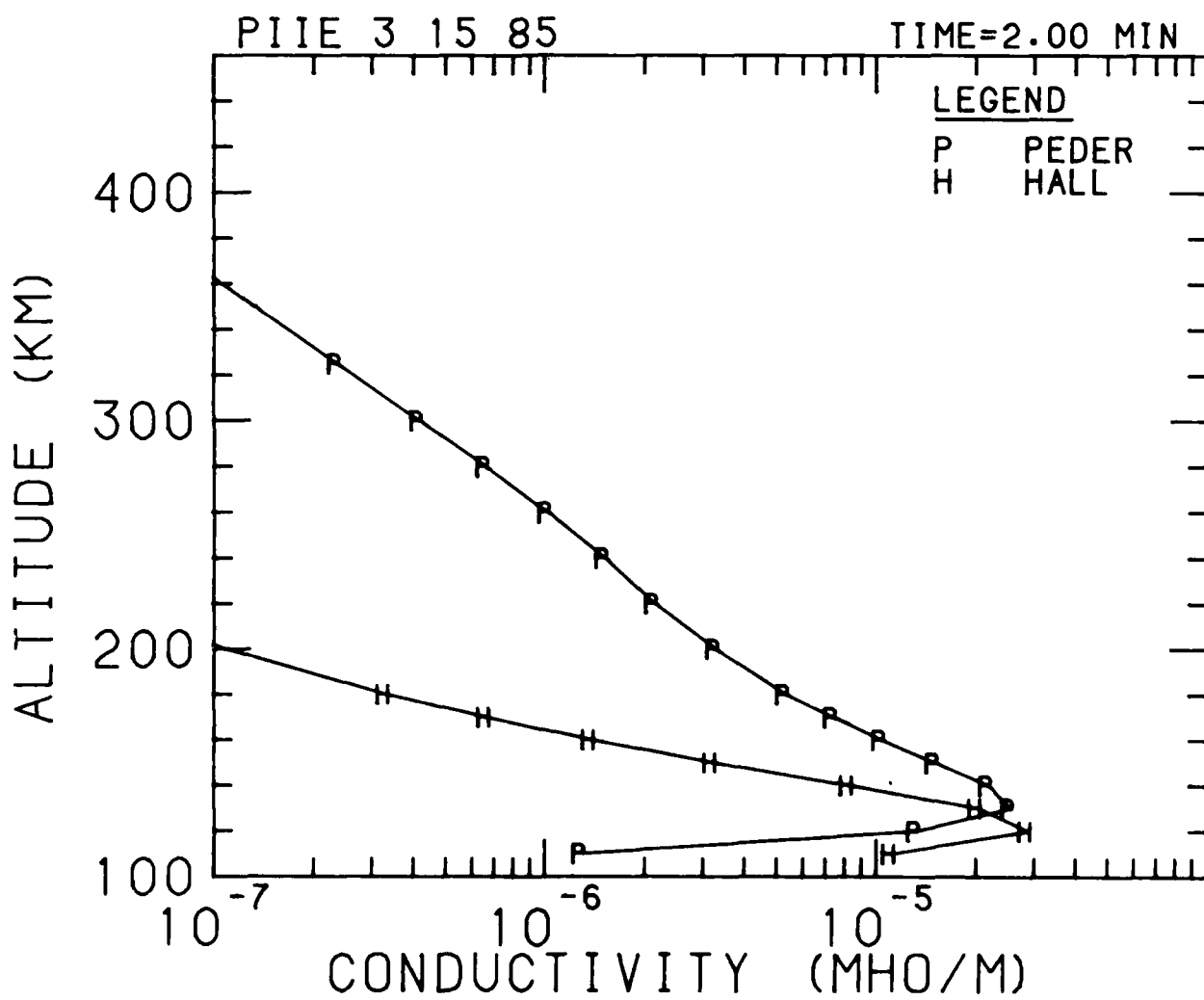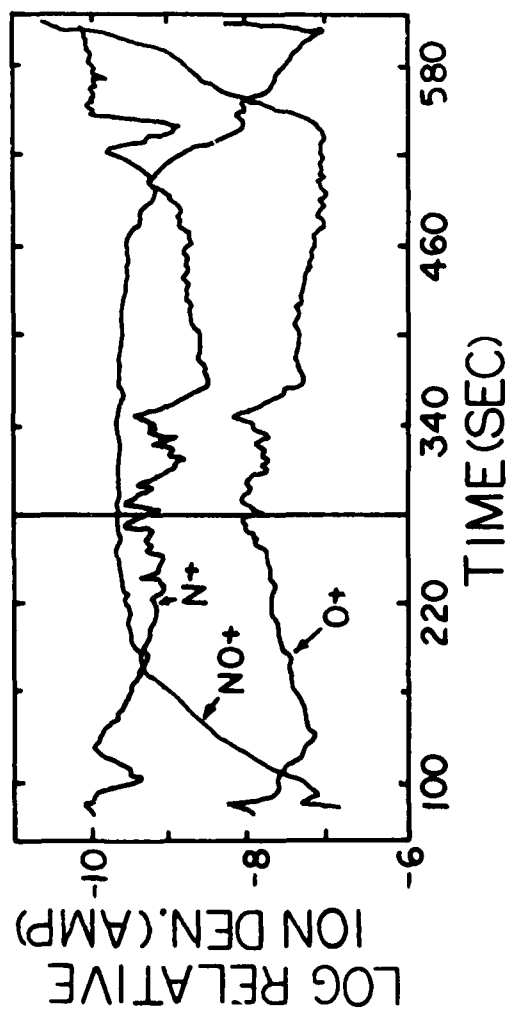
11

Figure 2

12

Figure 3

13

Figure 4

14

PIIE   3 15 85   TIME=2.00 MIN

Figure 5

15

PIIE 3 15 85   TIME=2.00 MIN

Figure 6

Figure 7

17

Figure 8

Figure 9

19

PIIE 3 15 85

LEGEND
⊕   1.00 MIN
△   2.00 MIN
+   5.00 MIN
✕   10.00 MIN
◇   15.00 MIN
✦   20.00 MIN
⧖   25.00 MIN
⧖   30.00 MIN

ALTITUDE (KM)

DENSITY (CM**-3)

Figure 10

20

PIIE 3 15 85

LEGEND
⊙	15.00 MIN
△	18.00 MIN
+	20.00 MIN
×	22.00 MIN
◇	25.00 MIN
✦	30.00 MIN

ALTITUDE (KM)

DENSITY (CM**-3)

Figure 11

21

PIIE 3 15 85

LEGEND
⊕	1.00 MIN
△	2.00 MIN
+	5.00 MIN
✕	10.00 MIN

Figure 12

22

Figure 13

PIIE 3 15 85 TN=750 K

Figure 14

24

PIIE 3 15 85 TN=1250K
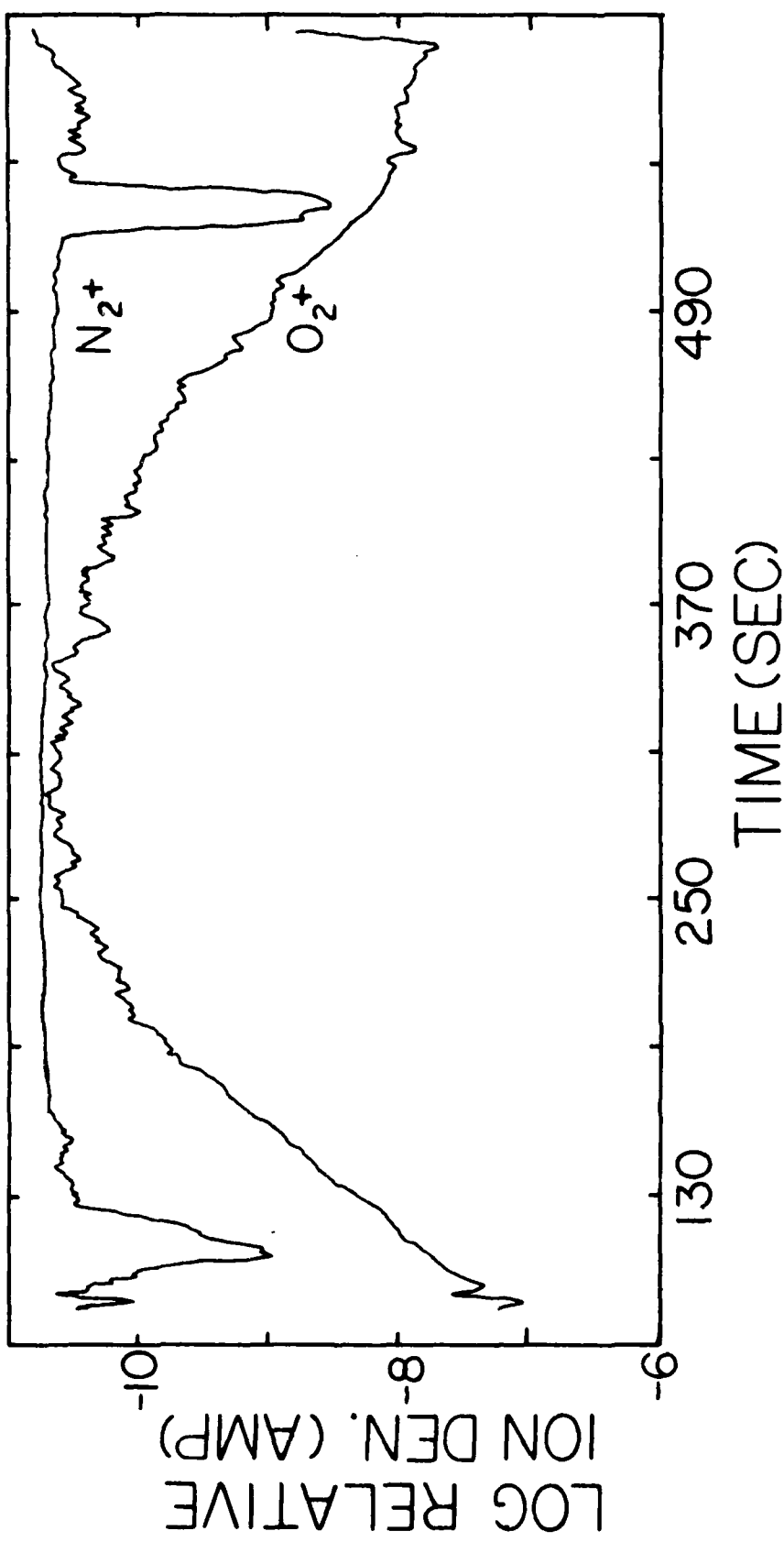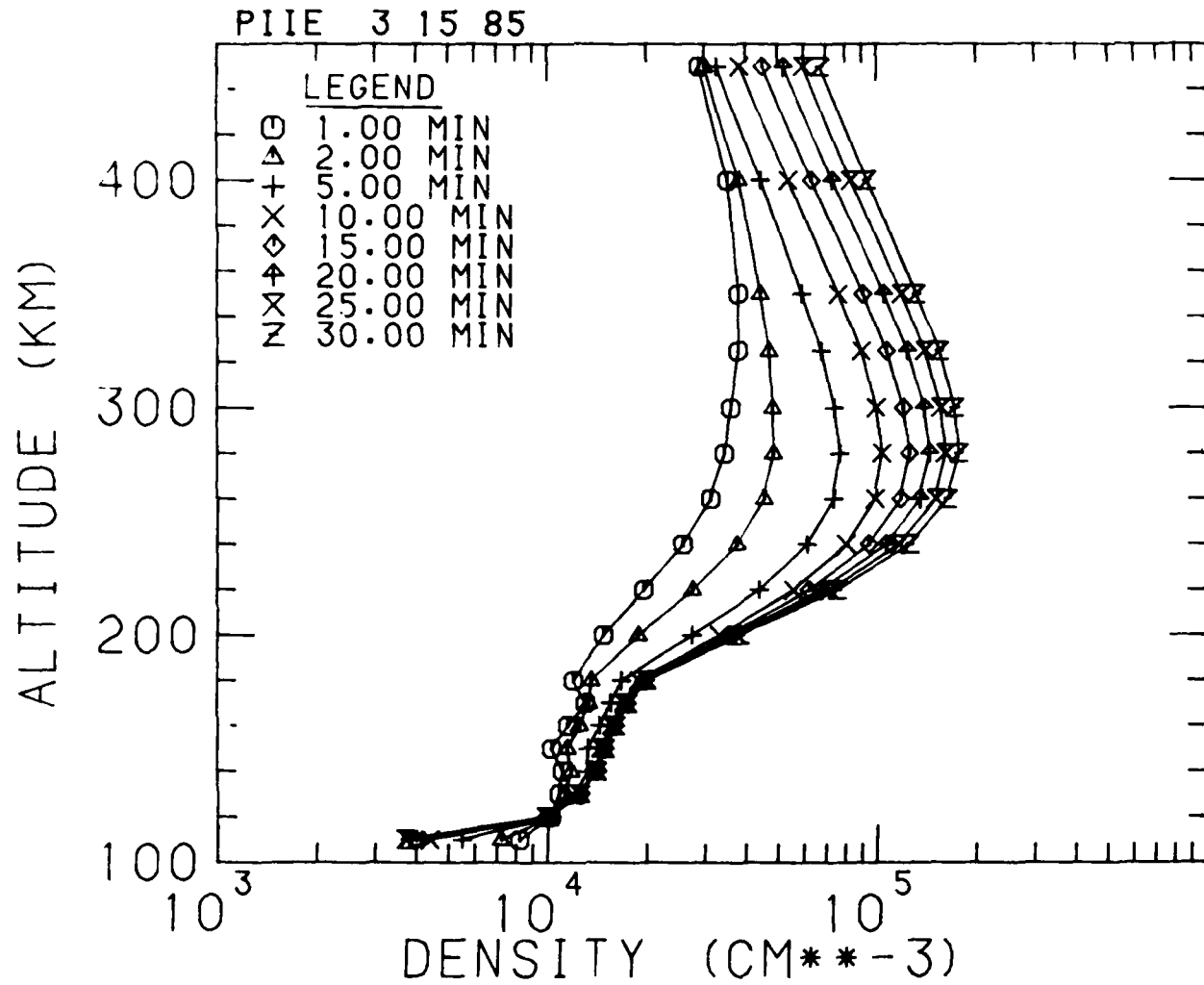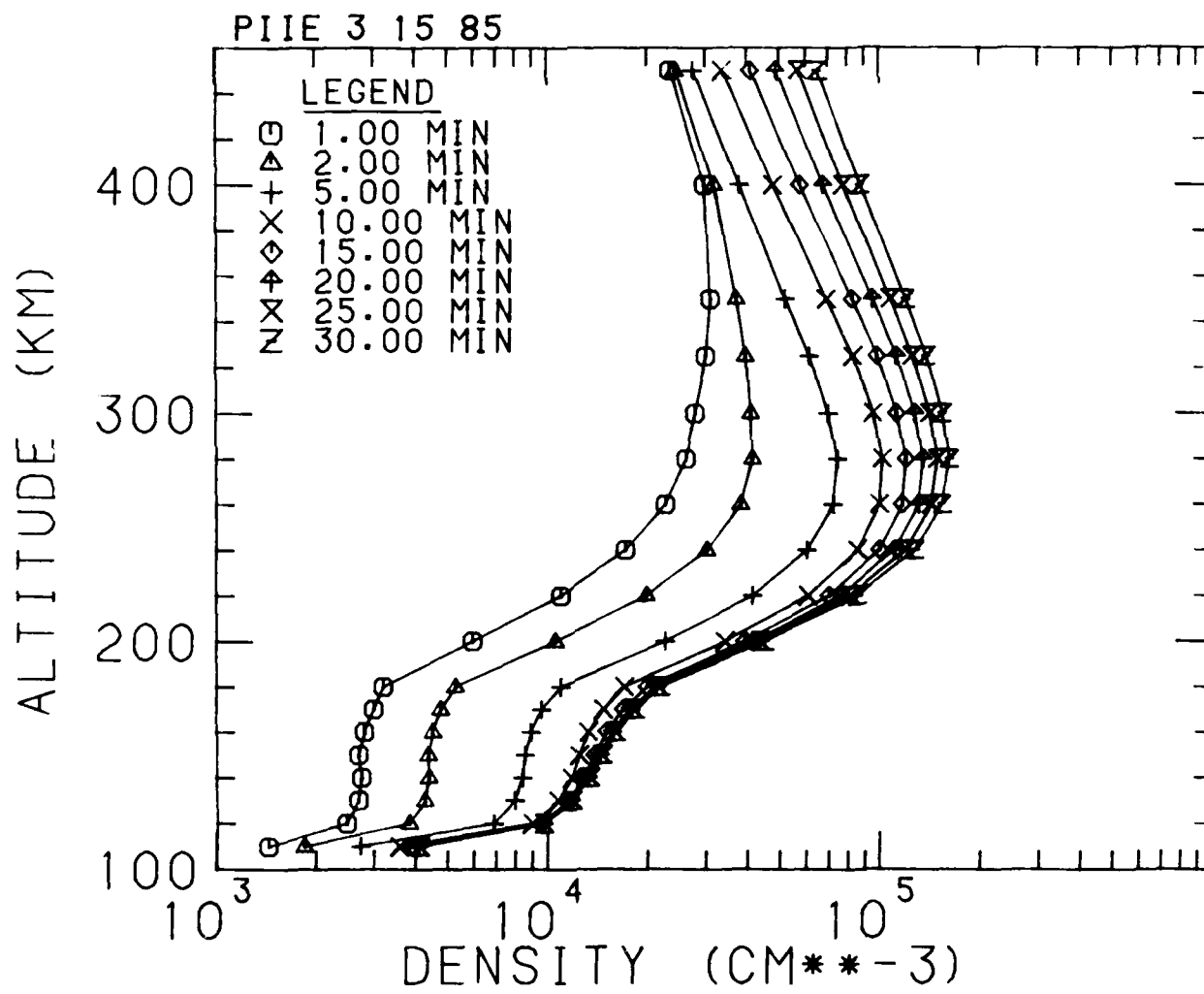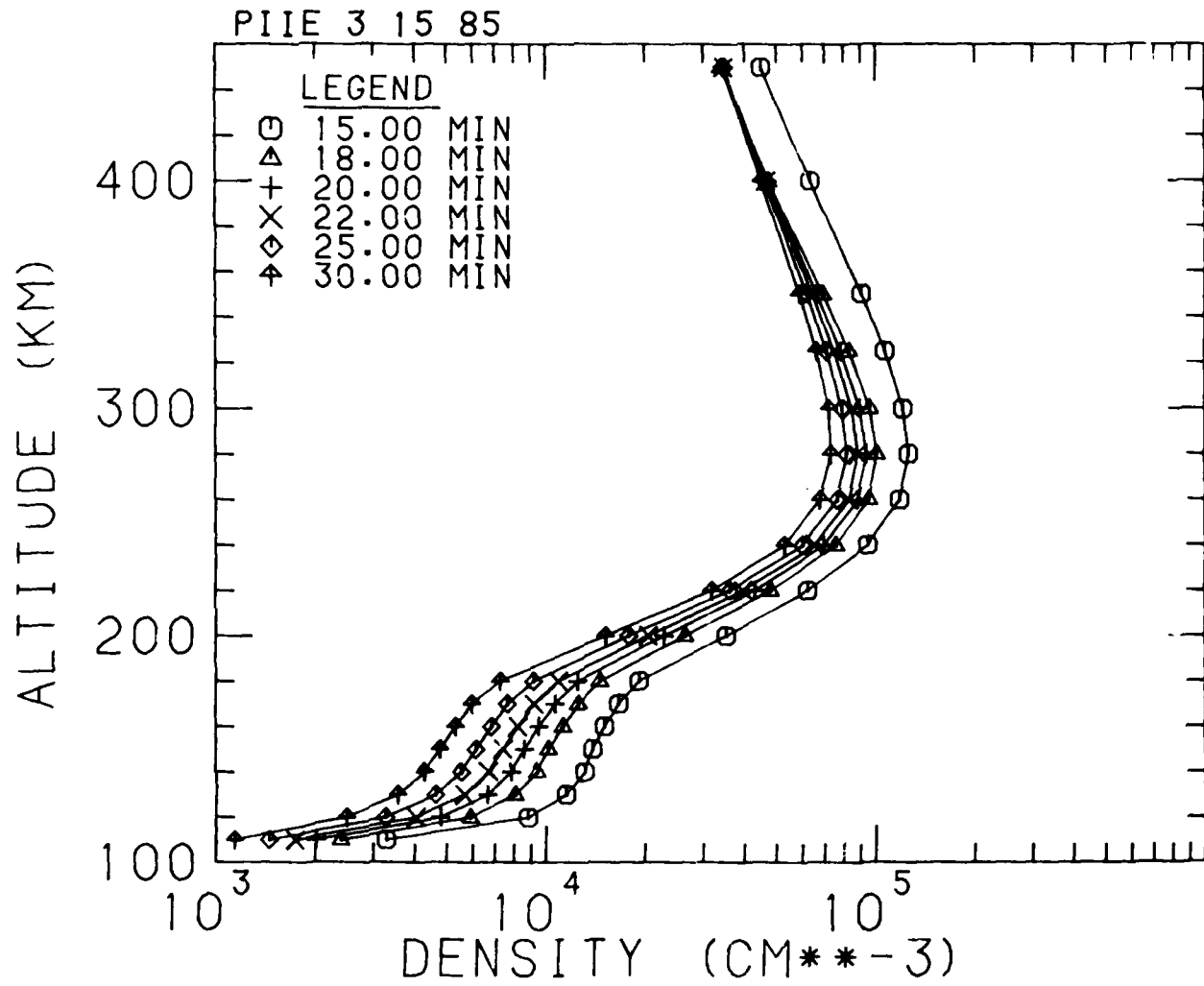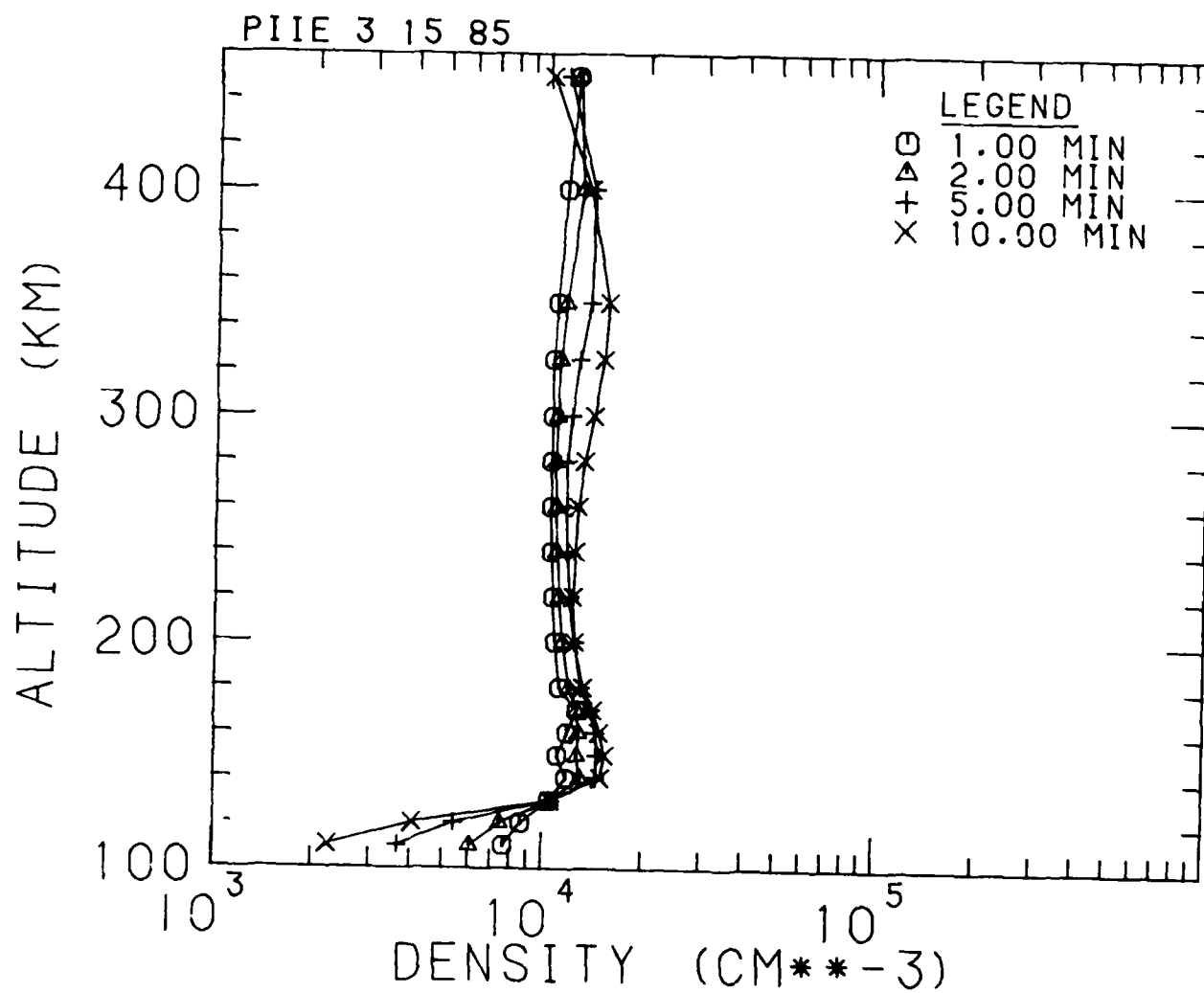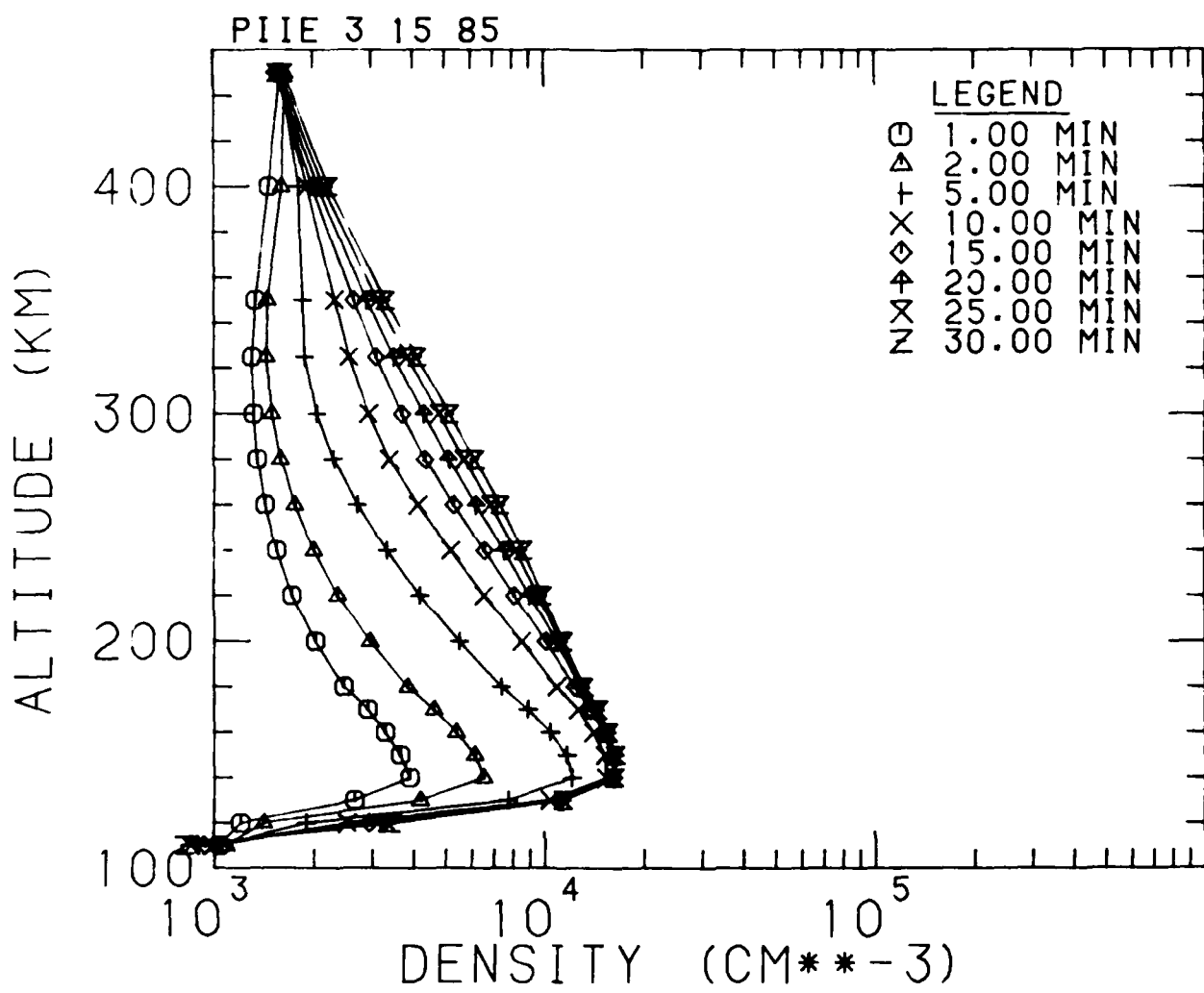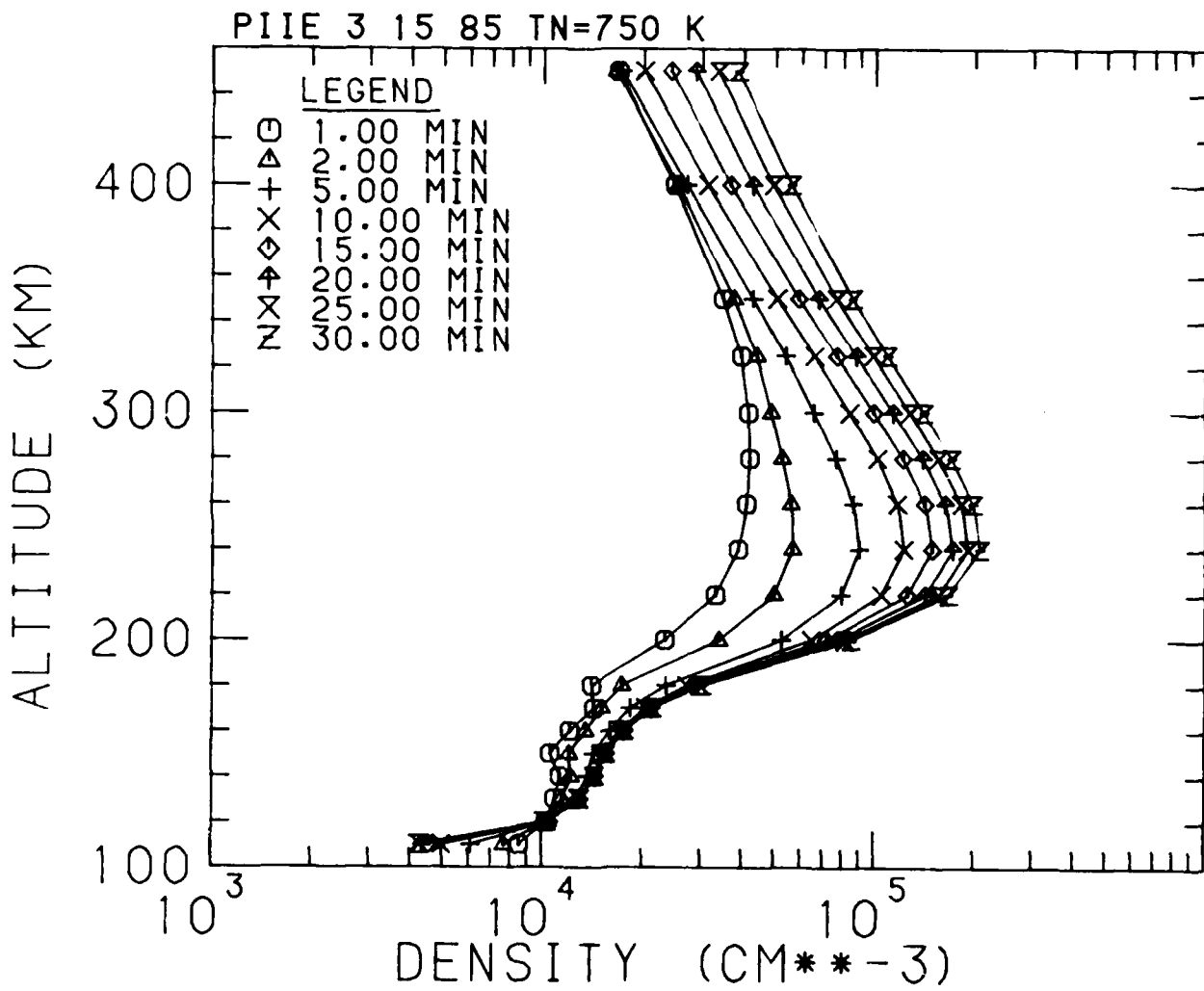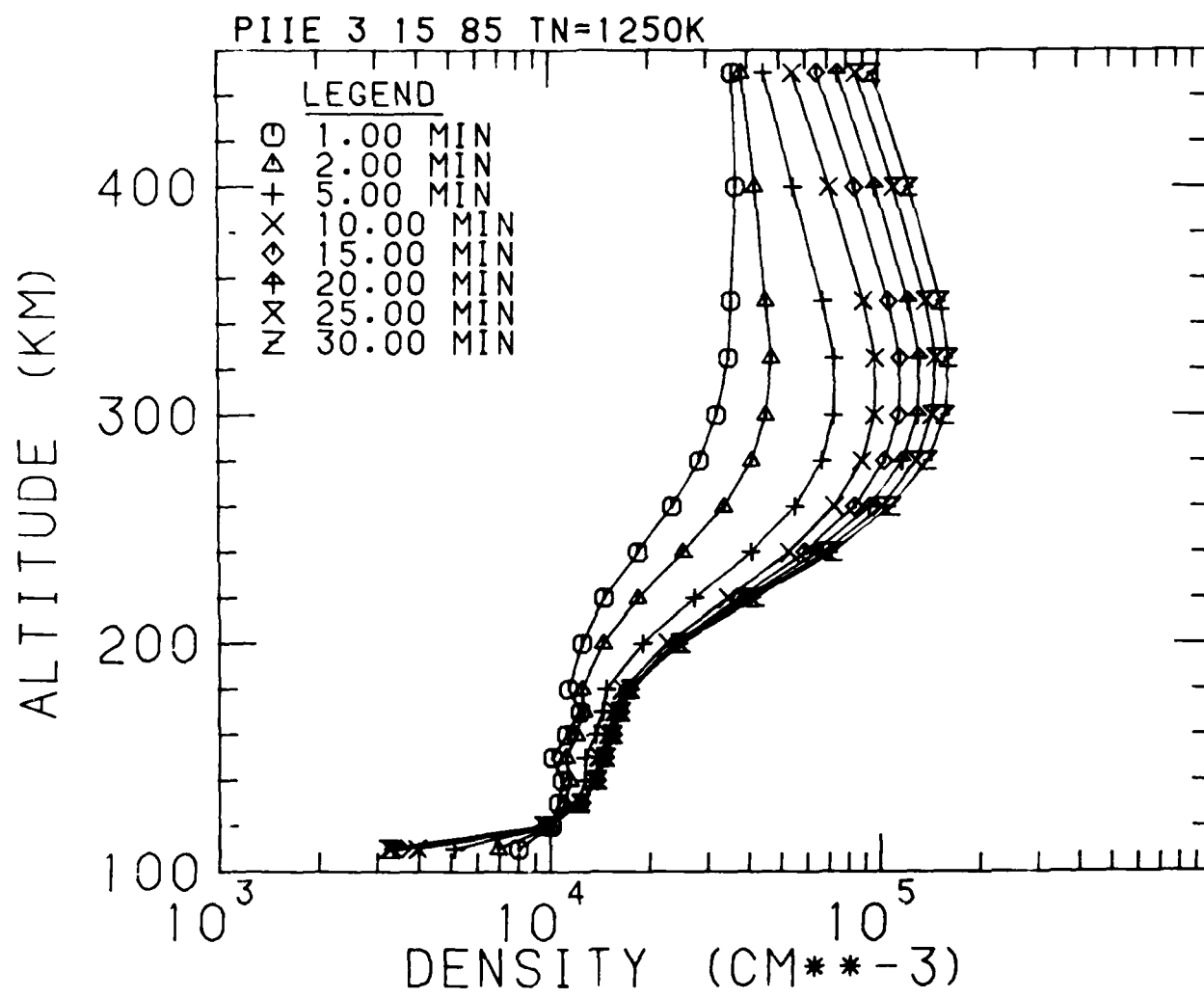
Figure 15

25

END

DATE
FILMED

6-88

DTIC